

Photographic response to x-ray irradiation. II: Correlated models

C. T. Chantler

In this paper models from the first paper are generalized so that they include the correlation of attenuation coefficients and coverages with emulsion depth. They avoid further assumptions and can provide physically meaningful parameters (as opposed to earlier studies); thus closer agreement with experimental measurements is obtained. The difficulty in estimating correlated overlap functions is discussed. Error estimates resulting from grain statistics are generalized and computed in a self-consistent manner. Contributions to granularity from densitometer and grain statistics have been shown to be significant or dominant in most emulsion types. The formulation derives reliable error estimates. Correlated models are important for thick emulsions such as DEF-392, whereas integral formalisms may be as useful for thin emulsions. In agreement with the first paper, reciprocity failure appears to be negligible for UV or x-ray energies above 9 eV.

1. Introduction

The photographic detection of x rays with 1–3- μm resolution creates a nonlinear density-intensity response. Semiempirical formulas reproduce local features of the density-intensity curve in controlled experiments,^{1–6} but parameters are of little physical significance. Extrapolation to other energies, densities, angles, or emulsions is often invalid. Accurate formulas are required for absolute and relative intensities of spectral features. They yield information on scattering processes and experimental parameters.

In this paper a framework is developed for linearization with uncertainties; it is based on earlier work⁷ and on the discussion in the previous paper,⁸ referred to hereafter as CI. Particular concern is focused on results for Kodak 101-07 and Kodak DEF-392 emulsions. Data in the literature for these emulsions relate to normal-incidence geometry and to diffuse or specular densities. Uncertainties in conversion factors can lead to significant errors in manipulated data at high densities, as addressed in CI. The conversion has been carried out as described in detail there, as required, with the calibration uncertainty specified.

When this work was performed the author was with Clarendon Laboratory, University of Oxford, Parks Road, Oxford OX1 3PU, England. The author is now with Quantum Metrology Division, National Institute of Standards and Technology, Gaithersburg, Maryland 20899.

Received 26 November 1991.

0003-6935/93/132398-13\$05.00/0.

© 1993 Optical Society of America.

Densities referred to herein are (experimental) specular optical densities from matched 0.1×0.1 numerical aperture optics, which is nearly identical to the ideal (theoretical) specular densities of the formulas presented. Although consideration of diffuse densities would necessarily involve discussion of multiple optical scattering within the emulsion, for any density, this has been avoided effectively by the above conversions for $D < 4$ or so, which covers the range of available data sets. Multiple optical scattering should play a minor role in the modeling presented here. Later developments may address this issue in more detail, which is discussed in Ref. 1.

Section 2 reintroduces standard parameters and the possible distortion of their values from their simple physical interpretation. In Section 3 we extend this to indicate regimes where the integral formalism of CI should fail, while a (correlated) summation model may yield significant improvement in agreement with experiment, with parameters of greater physical significance. Development of the latter model requires formulas for fractions of grains occluded or otherwise along the x ray (Section 4) and densitometer photon (Section 5) paths, which in turn requires an estimation of the pairwise correlation functions (Section 6). Improvement of the earlier error estimate is indicated in Section 7, where the equations of the sections above are used.

Comparisons of experiment with modeling are presented for DEF (Section 8) and 101 (Section 9) emulsions; both sets indicate the usefulness of this procedure and the range of applicability of this model

over energy, density, and emulsion type. Conclusions based on the significance of the introduced C_f and S_f parameters are explained in the later sections and summarized in Section 10.

Heterogeneous absorption coefficients are estimated for spherical grains rather than aligned cube models and for each layer rather than with the limit at deep layers for surface layers. This helps one to address earlier anomalies in the intensity-density relation. Application of these models is discussed in the next paper in this series.⁹

2. Clustering, Effective Coverage, and Critique of Integral Methods

The models from CI fitted the coverage per grain S and the cross section σ so that they were larger than spherical geometric grain cross sections σ_g , and the ratios of these quantities (S_f , C_f) were provided in Tables 4 and 5 (Sections 17 and 18). These parameters modify the maximum-density and low-exposure D/I ratio, respectively. Values reported by Henke *et al.*^{10,11} imply coverages of 2.4 and 5 per layer for different emulsions, in clear disagreement with data. In CI I discussed low coverage, low density, and other assumptions of the given formalism, which explain this distortion of parameters from physical bounds. In Table 1 the primary variables defined in CI or herein are summarized; they relate to the photo-

graphic response of emulsions to x rays. The models in CI [Eqs. (25a)–(25c)] yielded $S_f = 2.0$ – 2.4 and 1.5 for DEF and 101 emulsions, which may be larger than expected but are constrained by overlap considerations, which give coverages per layer of $M_0S \approx 0.94$ and 0.98 and hence effective mean values of $S_f \approx 1.6$ and 1.3 , respectively. Fitted values for C_f were 2.3 and 1.3 – 1.5 for the two films.

The mean grain diameter \bar{d} is well defined and in agreement with experimental measurement. If physical, the value of C_f suggests the chemical development of clusters of exposed and unexposed grains. This is common if the AgBr grains are platelike, needles, porous (fanlike), or of other nonspherical forms.¹¹ DEF shows almost uniformly spherical grains, which (with the gelatin) inhibits cluster aggregation. However, there is a grain size distribution, and the presence of varying sizes of grains aids this developable cluster formation.

If the value of S_f is due to development or flattening of grains during development, the ratio should remain constant at high exposures, as in the model. Developers (GBX and D-19) contain hydroquinone in an alkaline pH with a NaSO_3 preservative and Na_2CO_3 buffer (plus KBr and a developing agent). Micrographs of typical unexposed and developed grains are of similar shape and cross-sectional area (within a factor of 2).¹¹

Table 1. Summary of Primary Variables in This and CI

Symbol	Definition	Equation/Section	
		CI	This Paper
$I = I_p/A_d$	Exposure of radiation intensity (photons per square micrometers)		
D	Specular optical density	Eqs. (6), (25)	Eq. (12)
τ, τ_l	Optical transmission of film or layer	Eq. (3)	Eqs. (9), (11)
T, t_0, t_b	Emulsion, supercoat, and substrate thicknesses	Section 1	Eqs. (1), (6)
M_0	Grains per unit area, monolayer packing density	Eq. (2)	Section 2
M_l	Exposed grains per unit area in layer l	Eq. (2)	Section 2
\bar{d}	Mean AgBr grain diameter in emulsion	Eq. (3)	Section 2
d'	Mean path length through AgBr grain	Eq. (1)	Eq. (1)
μ_0, μ_1, μ'	Attenuation coefficients for gelatin, AgBr, emulsion	Sections 12–14	Eq. (1)
$\sigma_g = (\pi/4)\bar{d}^2$	Geometric grain cross section	Section 4	Section 2
σ	Effective cross-sectional area per grain	Eq. (1)	Section 2
S	Effective cross section of developed silver cluster	Eq. (3)	Section 2
$C_f = \frac{\sigma}{\sigma_g}, S_f = \frac{S}{\sigma_g}$	Cluster factor, cross-section increase on development	Section 17	Section 2
S_1	(Oblateness) shape factor common to C_f and S_f		Section 2
$\%v/v$	Mean volume fraction of AgBr grains in emulsion	Section 2	Section 2
$V_0 = \frac{4\pi}{3}\bar{d}^3$	Grain volume	Section 3	Section 3
V	Coverage of grains of film in (summation) half-layer		Section 3
$G_{tot\ i}, G_{tot}$	Grains per $\bar{d}/2$ x-ray/densitometry path length in area A_d	Eq. (11)	Sections 3, 5
h	Mean (lateral) separation of grain centers in emulsion	Section 8	Section 3
α, d_0, a, b	Semiempirical coefficients of earlier models	Section 2, Eq. (25b)	
C_1, C_2	Correlated grain fraction occluded by prior half-layers	Section 4	
J, d_y, z_m'	Integral and coefficients for absorption of x ray in grain	Eqs. (25), (30)	Section 4
$f_f(j)$	Grain fraction in half-layer j unoccluded by prior layers	Eqs. (1), (25)	Section 4
$f_o(j)$	Fraction of grain (area) occluded by half-layer j		Section 4
z, z_0, z_j	Exposure probability for depth x , surface, or half-layer j		Section 4
G_i, G_s, G	Estimates of number of exposed grains in emulsion	Section 4	Section 5
$Pl(i), V(i)$	Fraction, coverage of developed grains in half-layer i		Section 5

The apparent increase of S and σ can also be a function of the mean grain shape (oblateness of spheres, for example), which will increase the cross section and coverage per grain, and the number of layers involved. This shape factor is a characteristic of undeveloped grains and may be given by S_1 . This may occur at the 20% level but would be strongly correlated with $\%v/v$ and is at the level of precision of \bar{d} . It is assumed here that such an effect is included in the other variables.

These values may also be due to distortion from physical bounds by inadequate formulation of the density-intensity relation. The assumption of low coverage and shadowing retained only for the first few M_0S terms in the expansion and attempted to treat the first layer with a different form [Eqs (25a) and (25c) in CI] or include an empirical constant d_0 to allow for effects in the first few layers [Eq. (25b) in CI]. The heterogeneous attenuation coefficient μ' is not constant with grain depth but increases to the limiting value after the first few layers. Although $M_0\sigma_g$ is constant with depth and M_0S is roughly constant for high energies and low attenuation, or for low densities, the latter increases with depth as a function of exposure. The models of CI integrate over depth and assume M_0S to be constant, which is false and will fail in some regimes.

3. Correlation of Grain Positions and Half-Layer Summation

The centers and exposed areas of grains well separated in the emulsion will be independent of higher or lower layers. Conversely, if grains are uniform in size and close-packed, full exposure of the first three layers will occlude all light. The occluded fraction for the first layer would then be a maximum of 0.907 (assuming that $S = \sigma_g$) with the second and third layers contributing 0.0415 each in this high-exposure limit, with no further contribution from underlying layers. Factors sum, rather than the multiplication of transmissions in the models. This would correspond to transmission factors of $0.093 = 1 - M_1S$ for each of the first three layers (the remainder being irrelevant) and overall transmission of 8×10^{-4} or $D \approx 3.1$ (instead of 0 and ∞ , respectively).

In such correlated cases, saturating densities may exceed model predictions, so that linearized intensities for peaks may be overestimated. Errors may dominate at densities above 2.5, and large scatter is observed above densities of 2.0 (partly from densitometry rather than the model).¹¹ The thick emulsion of DEF film involving an estimated eight layers minimizes this by increasing the effect of deep layers. The effect of deeper levels is never greater than that possible from the correlation of surface layers but will approach the latter.

The shadowing of grains is less negatively correlated for $\%v/v = 0.40$ (DEF) compared with the extreme given above; hexagonal close packing would give $\%v/v \approx 0.74$ while simple cubic packing gives $\%v/v = (\pi/6) \approx 0.524$. DEF-392 and other films

may be modeled by loose cubic packing.⁵ The correlation depth (the depth over which the disposition of centers is negatively correlated) is \bar{d} , but on average there is only one grain in this depth. Grains at lower depths may be positively correlated (simple cubic packing) or negatively correlated [e.g., hexagonal or loose body-centered cubic packing], and the amorphous nature of the emulsion should average this to zero. A random distribution of grains in body-centered cubic packing in the allowed space implies depths of consecutive grains of different monolayers to be $\ll \bar{d}/\sqrt{3} \approx 0.58\bar{d}$. There the projections of the centers will lie at distances of $\sqrt{(2/3)}\bar{d} \approx 0.82\bar{d}$ from one another, and occlusion by a lower layer should contribute more to density than in earlier models. This contributes low probability compared with slightly larger depths with less correlation, but the overlap is significant for all densities and is larger for developed clusters with $S_f \gg 1$.

In CI I considered a half-layer summation for estimating grain statistics (Section 4). This may be preferred over a layer summation since z varies less over a half-layer and there is the potential for allowance of overlap. It also permits variation in the coefficients with depth and nonindependence of contributions from adjacent elements, as opposed to integral formalisms. A summation is now performed in steps *along the path length of the x ray*; thus "sin θ " appears in the number of layers and not in the depth. The coverage of grains with centers in this reduced depth is $C = M_0\sigma_g \sin \theta$, but the occlusion from adjacent grains or adjacent parts of the same grain is $C/\sin \theta$. Equivalently, for I_p photons incident on the surface area A_d ,

$$\frac{I_p \sigma_g}{A_d \sin \theta}$$

of these will pass through a given spherical grain, but photons passing through this area will also pass through $M_0/(\sin \theta)$ grains in the coverage depth. Densitometry is at normal incidence, so this is relevant only for the evaluation of coverages and attenuation.

Grains of similar size in the upper half of the first monolayer cannot overlap one another; thus the coverage of the film (irrespective of clustering) because of this depth is

$$V = G_{\text{tot}} \frac{\sigma_g}{A_d} = \frac{\%v/v}{V_0} \frac{\bar{d}}{2} \sigma_g.$$

If the development increases S significantly beyond σ_g , M_0S will be increased to a value of less than unity. Flattened silver clusters can overlap over depths that are $\ll \bar{d}/2$, unlike the grains; thus it is possible but unlikely that the true S_f could give $V \gg 1$ over a half-layer. In the case of DEF and 101 emulsions, $V = 0.3$ and 0.56 ; thus this assumption is equivalent to $S_f < 3.3$ and $S_f < 1.79$, respectively. This is borne out in the sections below and in CI.

In CI and this paper it is assumed that the devel-

oped coverages per half-layer may be given by $V S_f$. This is correct for $h > \bar{d} S_f$ or $S_f < 2.6$ (DEF), $S_f < 1.4$ (101), but increasingly inaccurate otherwise. This is good for DEF but may introduce a slight distortion of S_f for 101, from an actual coverage increase on development per grain to an *effective* increase. The half-layer summation ensures that this is correct for any emulsion for grains before development. The grains in the next half-layer are negatively correlated with this layer. (They fill the holes so that $M_0 \sigma_g$ for the layer of $\approx 2V = 0.6$, but correlation is not 100%; thus 0.57 is more accurate.)

The attenuation coefficient is typically μ_0 over the path length and neither μ_1 nor μ' as defined in CI. For deep layers the coefficient approaches the heterogeneous mean, but for the first few layers each grain will have a significant fraction of its surface exposed on a direct path to the surface with *no* intervening grains. Those grains with a larger fraction exposed will have a much greater incident intensity per grain, and hence, in a correlated way, they are more likely to be exposed and to occlude a larger region than the mean absorption coefficients suggest.

4. Grain Fractions

The correction of the problem lies in estimating the average fraction of each grain with such a direct path. Since each half-layer is correlated to the next, a fraction $C_1 < V$ of grains in every half-layer will be occluded by the next. Of the remainder, each other higher half-layer will occlude a fraction $f_o(j)$ equal to V times the fraction $f_f(j)$ of grains receiving a direct path from the surface (Fig. 1). This latter estimate neglects second-order correlation C_2 between grains whose front surfaces are separated by two half-layers.

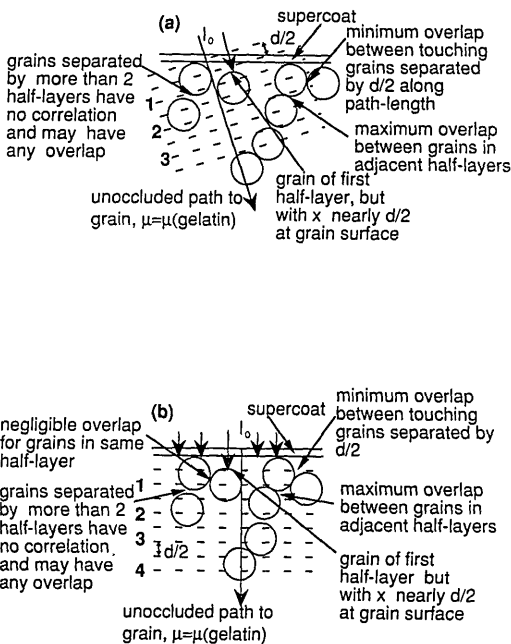


Fig. 1. Thick emulsion model illustrating correlated overlap and transmission functions between half-layers for (a) incident x-ray and (b) densitometry photon paths.

Second-order correlation depends on interunit forces, which are positive for simple cubic lattices and negative for body-centered cubic or hexagonal close-packing ordering. Here, such forces are nonexistent, and the relative spacing and ordering are random (within the allowed volume). They give a small positive correlation that is an order of magnitude less than the first-order correlation between half-layers, which makes a small contribution to absorption and density. This is especially true for emulsions with low packing densities of grains.

Of the fraction occluded by the preceding half-layer, $f_o(j-1)$ will be occluded only by the edge of those grains and hence will have a reduced mean path length of $\approx \bar{d}/2$ through the crystal; the remaining fraction will be occluded by earlier layers. This yields three absorption coefficients and probabilities contributing to the probability of exposure per grain, so that relative to the surface (zeroth) layer [with Eqs. (1) and (8) of CI]

$$\begin{aligned}
 z_0 &= \frac{I_p}{A_d} \sigma [1 - \exp(-\mu_1 d')] \\
 &\quad \times \exp(-\mu_0 d_y) \exp(-\mu_0 t_0 / \sin \theta) \\
 &= I_{inc} \sigma [1 - \exp(-\mu_1 d')] \exp(-\mu_0 d_y), \quad (1) \\
 z_j &= z_0 \left(f_f(j) \exp[-\mu_0(j+0.5)\bar{d}/2] \right. \\
 &\quad \left. + \left[\sum_{k=0}^{j-3} f_o(k) + f_o(j-2) \right] \right. \\
 &\quad \times \exp\left\{-[\mu'(j-0.5) + \mu_1] \frac{\bar{d}}{2}\right\} \\
 &\quad \left. + f_o(j-1) \exp\{-[\mu_0(j-0.5) + \mu_1] \bar{d}/2\} \right). \quad (2)
 \end{aligned}$$

Following CI, Sections 11, 12, and 15, one should apply the scattering and photoelectron considerations of Eq. (26) therein; the mean factor for $[1 - \exp(-\mu_1 d')] \exp(-\mu_0 d_y)$ is given by J in Eq. (30), and the estimate of $\bar{d}/4$ for the mean distance from the bottom of the supercoat to the front of the first grain surface should be replaced by forms following z_m' in Eqs. 25(a) and 25(c). This has been mentioned elsewhere⁷ where an approximate intermediate value for J was used. With these corrections Eqs. (1) and (2) become

$$\begin{aligned}
 z_j &= z_0 \left(f_f(j) \exp(-\mu_0 j \bar{d}/2) + \left[\sum_{k=0}^{j-3} f_o(k) + f_o(j-2) \right] \right. \\
 &\quad \times \exp\left\{-[\mu'(j-1) + \mu_1] \frac{\bar{d}}{2}\right\} \\
 &\quad \left. + f_o(j-1) \exp\{-[\mu_0(j-1) + \mu_1] \bar{d}/2\} \right) \\
 &= z_0 [a_1(j) \text{Abs}_1(j) + a_2(j) \text{Abs}_2(j) + a_3(j) \text{Abs}_3(j)], \quad (3a)
 \end{aligned}$$

$$z_0 = \frac{I_p}{A_d} \sigma J(\mu + \sigma_{\text{scat}} + \delta_{\gamma-e}) J_m',$$

$$J_m' \approx \begin{cases} 1 & \text{rough emulsion} \\ \frac{2 \sin \theta}{\mu_0 \bar{d}} \{1 - \exp[-\mu_0 \bar{d}/(2 \sin \theta)]\} & z_0/J_m' < 1, \text{ smooth.} \\ \exp[-\mu_0 \bar{d}/(4 \sin \theta)] & z_0/J_m' > 1, \text{ smooth} \end{cases} \quad (3b)$$

Grains in the first half-layer have μ_0 as the attenuation coefficient. As the free fraction decreases and contributions are dominated by occluded fractions, deep layers have attenuation coefficients approaching μ' . Free fraction coefficients are rigorous, use of $\bar{d}/2$ for the last half-layer occlusion is a good approximation, and use of $\mu'(j-1) + \mu_1$ in the occlusion of higher layers is less precise. For deep layers replacement of the latter by $j\mu'$ is more reasonable and approaches the uncorrelated limit.

Note that $f_0(j-1) \leq C_1$ since a fraction of C_1 , occluded by the preceding layer, will already be occluded by some other layer. The sum of the three fractional coefficients is unity (the whole grain); thus

$$f_f(j) = 1 - \sum_{k=0}^{j-1} f_0'(k),$$

$$f_0'(k) = \begin{cases} VS_f f_f(k) & k < j-2 \\ C_2 f_f(k) & k = j-2, \\ C_1 f_f(k) & k = j-1 \end{cases} \quad (4)$$

where $S_f = 1$ here, since we are dealing with grains and not silver clusters. This gives recursion formulas for the coefficients. The additional fraction of area occluded by each half-layer is

$$f_{O,\text{area}}(k) = (S_f)V f_f(k). \quad (5)$$

For $k = j-1, j-2$ this is not equal to the fraction of the grain occluded because of the positive or negative correlation. If applied as $f_0'(k)$ in Eq. (4), this would underestimate the coverage of a series of layers (and hence the density) because of the dominant negative correlation of C_1 . The third-order correlation is important for close-packed or regular stacking arrangements; but for liquids and noncrystalline aggregates such as the emulsion, higher terms rapidly approach V .

Since the dominant photographic response for soft x rays is in the first few layers and the dominant free-path coefficients are roughly

$$f_f(j) = \left(1 - \sum_{k=1}^{j-1} C_k\right)$$

for these half-layers, any coefficients of similar form will provide grain number and density estimates even if iteration of the (wrong) recursion relation leads to

negative coefficients for deeper layers. For large exposures this is more serious and leads to density errors. With the correct recursion relation above, these errors are contained in inaccuracies in the estimation of C_1 and C_2 with possible neglect of higher terms. A simple approximation is to use Eq. (4) but transfer to Eq. (5) for the evaluation of layers when these errors accumulate and yield maximum coverages that are greater than unity.

5. Grain and Density Estimates

The grain estimate and error may be evaluated directly with Eq. (11) of CI, with the sum now over $(2T/\bar{d} - 1)/\sin \theta$ half-layers and the scaling V replaced by the total number of grains per path length $\bar{d}/2$ at this angle or

$$G_{\text{toti}} = V \frac{A_d}{\sigma_g} \sin \theta = \frac{\bar{d} \rho v / v}{2V_0} A_d \sin \theta, \quad (6a)$$

$$G = G_{\text{toti}} \sum_{j=0}^{\text{int}\{(2T/\bar{d}-1)/\sin \theta\}} [1 - \exp(-z_j)]$$

$$\pm \left\{ G_{\text{toti}} \sum_{j=0}^{\text{int}\{(2T/\bar{d}-1)/\sin \theta\}} [1 - \exp(-z_j)] \right. \\ \left. \times \exp(-z_j) \right\}^{1/2}. \quad (6b)$$

For deep layers the density approaches Eq. (12) in CI with the effective reduction of S_f ; but for low exposures it approaches $D = -\log_{10}[1 - S_f \sum_j V(j)]$ because exposed, covered areas will tend not to overlap. This sum should also be given in half-layers; but this is different from the grain summation because the densitometer views at normal incidence. Correlation lengths and coefficients $a_1(i), a_2(i), a_3(i)$ are as for the x-ray path but must be reevaluated since each step of $\bar{d}/2$ corresponds to a maximum coverage of VS_f (i.e., $\times S/\sigma_g$ with grain number $G_{\text{tot}} = G_{\text{toti}}/\sin \theta$). The mean fraction of developed grains in each half-layer may then be given from the earlier fractions through the path length as

$$Pl(i) = \sum_{j=\text{int}(i/\sin \theta)}^{\text{int}[(i+1)/\sin \theta]} a_j P_j$$

$$\pm \left[\frac{\sum_{j=\text{int}(i/\sin \theta)}^{\text{int}[(i+1)/\sin \theta]} a_j P_j (1 - P_j)}{G_{\text{tot}}} \right]^{1/2},$$

$$P_j = 1 - \exp(-z_j), \quad (7)$$

$$\alpha_j = \begin{cases} \sin \theta & \frac{i}{\sin \theta} \leq j, \frac{i+1}{\sin \theta} \geq j+1 \\ (j+1)\sin \theta - i & j < \frac{i}{\sin \theta} \\ i+1-j\sin \theta & j+1 > \frac{i+1}{\sin \theta} \end{cases} \quad (8)$$

For the values of exposed grain densities M_0 varying from layer to layer and for the increased cross section $S = S_f \sigma_g$, we must recalculate coefficients $C_1(i)$ and $C_2(i)$ using $V(i) = Pl(i)V$ for each half-layer giving the mean separation of cluster centers. Representing each exposed grain by an average grain leads to the (correlated) transmission factor

$$\tau = 1 - \left\{ \sum_{i=0}^{\text{int}(2T/d-1)} V(i)[1 - a_4(i) - a_5(i)] \right\} \quad (9)$$

from Eq. (5), where the coefficients correspond to $a_2(i)$ and $a_3(i)$ above, representing the fractions of each silver cluster occluded by grains in earlier layers and by the previous half-layer, respectively. No absorption factor is present: A grain fraction is (assumed) sufficient to absorb all incident visible light in the densitometer scan. Coefficients could be given by the mean occlusion from preceding layers, if we assume full occupation times the occupation probabilities: but this is inadequate, and the occlusion of each layer is computed separately. Only exposed grains contribute, so the free and occluded fractions vary through the half-layers, as does C_1 . Following Eq. (4), this then gives

$$\begin{aligned} a_4(i) &= \sum_{k=0}^{i-2} f_O(k), & a_5(i) &= f_O(i-1), \\ f_f(j) &= 1 - \sum_{k=0}^{j-1} f_O(k), \\ f_O(k) &= \begin{cases} V(k)S_f f_f(k) = VS_f Pl(k) f_f(k) & k < j-2 \\ C_2(k) f_f(k) & k = j-2 \\ C_1(k) f_f(k) & k = j-1 \end{cases} \end{aligned} \quad (10)$$

Errors are summed in the usual way, although $Pl(k)$, $k < i-2$ components in $a_4(i)$ and $a_5(i)$ have negative correlation with earlier contributions. There are two regimes, the first where correlated relations [Eq. (4)] are used and the second where uncorrelated forms [following Eq. (5)] are implemented. This transition is determined by the high-density calculation as above; at low densities the transition half-layer could be of greater depth, but the relation would not generally be smooth. The effects on C_1 and C_2 of $Pl(k)$ are neglected. The variance in τ (after layer l) is then

$$\begin{aligned} \text{er } \tau_l^2 &= \sum_{i=0}^l \left[\frac{VS_f f_f(i)}{Pl(i)} \right]^2 \text{er } Pl(i)^2 T^{*2}(l-i), \\ T^*(i) &= T^*(i-1) - T^*(i-2)Pl(l-i+2)VS_f, \\ T^*(0) &= T^*(1) = 1, \end{aligned} \quad (11a)$$

where $T^*(i)$ is equivalent to $f_f(i)$ but applied to half-layers in reverse order, neglecting effects of $Pl(i)$ on C_1 and C_2 . For uncorrelated half-layers, relative

errors add quadratically:

$$\text{er } \tau_l^2 = \left(\frac{\text{er } \tau_{l-1}^2}{\tau_{l-1}^2} + \frac{\text{er } Pl(l)^2 V^2 S_f^2}{(1 - Pl(l)VS_f)^2} \right) \tau_l^2. \quad (11b)$$

Finally the density is given by

$$D = \frac{-1}{\ln 10} (\ln \tau \pm \{\ln \tau - \ln[\tau + \sigma(\tau)]\}). \quad (12)$$

Equation (9) uses average grains where grains completely unoccluded in the path of the x ray (or completely occluded) will on average contribute to a decrease in transmission equivalent to the free fraction for that layer. For exactly normal incidence (the experimental data of Refs. 9–12) this may easily be false: The x ray and densitometer photon follow the same path; so an already occluded grain contributes 0 while a completely free grain contributes an area $S \approx \sigma_g S_f$.

At (1) low exposures or (2) angles below $\sim 75^\circ$, these equations are recovered, since (1) all grains have typically negligible occlusion or (2) adjacent half-layers (and hence the first two half-layers) have negligible occlusion, and all higher layers for $\theta \approx 45^\circ$ have the x ray and photon following different and uncorrelated paths. The latter argument implies that the equations above are valid for the case outlined in a subsequent paper; the former indicates where Henke's data and fitting parameters may be used to test these relations.

For high densities at normal incidence, coefficients may be modulated by the probability of obtaining a given fraction of the grain free in a given half-layer with the consequent reduction of transmission. Even then the development introduces a shift of up to a grain diameter of the exposed cluster and alters the shape—so these equations will still be valid to high precision.

6. Grain Overlap Correlation Functions

The mean occlusion of the previous half-layer C_1 propagates through the correlation and absorption coefficients. A corresponding uncertainty can lead to errors at high densities. One may estimate C_1 by noting that the mean separation of depths of grain centers in adjacent half-layers is $\bar{d}/2$, at which the minimum separation of centers in the horizontal plane is $0.866\bar{d}$, which corresponds to a maximum C_1 of 0.0577. The probability of the separation of depths

$$P\left(\Delta x = \frac{d_1 - d_2}{\bar{d}}\right)$$

is, for random arrangement, given by the available volume. This is the range of depths (of a grain) over which this separation is possible (given that the front surface of each grain lies in its respective half-layer), multiplied by the area available without grain superposition.

This area depends on nearest neighbors and their

angles and depth distributions, but the dependence is small. For a half-layer with mean area coverage of $V = 0.3$ (DEF) and centers arranged locally in a square, the adjacent grains are separated by

$$h = \sqrt{\frac{\pi \bar{d}}{V}} = 1.618\bar{d};$$

for an equilateral triangle the separation is slightly increased to $h = 1.7387\bar{d}$; and for grains clumped in pairs in squares $h = 2.2879\bar{d}$. Different incident angles and surface regions, together with C_f values, have no effect on C_1 . Use of a square arrangement assumes two fixed angles (or two fixed grain locations) given the available area (Fig. 2). This may be generalized to a parallelogram with only one fixed grain location. Larger values of h correspond to smaller mean values of C_1 because the fraction of available area outside the overlap distance \bar{d} ($C_1 = 0$) is increased. Taking the smaller value for a square arrangement, a minimum value of the horizontal distance between a corner of one layer and the grain center of the lower layer becomes

$$h_{r \min}(\Delta x) = \bar{d}[1 - (\Delta x)^2]^{1/2}, \quad (13a)$$

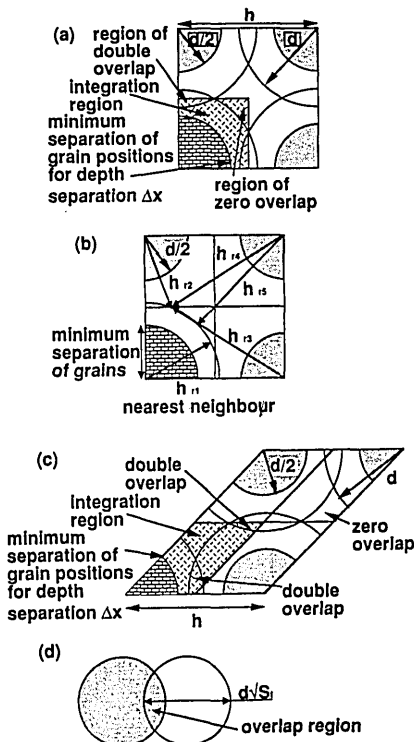


Fig. 2. Simple model for correlated overlap calculation when four near neighbors in the upper half-layer with mean spacing h , mean grain diameter \bar{d} , and a difference in depth of the underlying grain with its nearest neighbor given by $\Delta x = (d_1 - d_2)/\bar{d}$ are assumed, (a) and (b) relate to the square arrangement of neighbors, discussed in the text, versus a more general but less defined parallelogram arrangement of (c). (d) Overlap of grains.

corresponding to

$$C_1(h_r) = \begin{cases} \frac{2\theta}{\pi} - \frac{2h_r \sin \theta}{\bar{d}\pi\sqrt{S_f}} & h_r < \bar{d}\sqrt{S_f} \\ 0 & h_r > \bar{d}\sqrt{S_f} \end{cases},$$

$$\theta = \arccos\left(\frac{h_r}{\bar{d}\sqrt{S_f}}\right) \quad (13b)$$

and yielding an available area

$$A(h_r) = \begin{cases} \frac{h^2}{4} - \frac{\pi h_r^2}{4}, (\theta_1 = 0) & 0 < h_r < \frac{h}{2} \\ \frac{h^2}{4} (1 - \tan \theta_1) - \frac{h_r^2}{4} (\pi - 4\theta_1), & \\ \theta_1 = \arccos\left(\frac{h}{2h_r}\right) & \frac{h}{\sqrt{2}} > h_r > \frac{h}{2} \end{cases} \quad (13c)$$

On average one grain will lie in each square with symmetry requiring only the nearest neighbor (one quarter of the square) to be considered. Shadowing by next-nearest neighbors may be estimated for larger radii with

$$C_1(h_r)' = \begin{cases} C_1(h_r) + \frac{\theta_{\min 1} - \theta_1}{\frac{\pi}{4} - \theta_1} \frac{C_1(h_{r2})}{2} & \theta_{\min 1} < \frac{\pi}{2} - \theta_1 \\ C_1(h_r) + C_1(h_{r2}) + C_1(h_{r3}) + \frac{C_1(h_{r4}) + C_1[(\sqrt{2})h - h_r]}{2} & \theta_{\min 1} > \frac{\pi}{2} - \theta_1 \end{cases},$$

$$h_{r2} = \begin{cases} h_r & h_r > h/2 \\ h - h_r & h_r < h/2 \end{cases},$$

$$h_{r3} = (h^2 + h_r^2 - 2hh_r \sin \theta_1)^{1/2},$$

$$h_{r4} = (h^2 + h_{r2}^2 - 2hh_{r2} \sin \theta_1)^{1/2},$$

$$\theta_{\min 1} = \arccos\left(\frac{h_r^2 + h^2 - S_f \bar{d}^2}{2h_r h}\right). \quad (13d)$$

The nearest grain overlap is always at distance h_r , the second and third grains in this arrangement vary in horizontal distance from h_{r2} to h_{r3} , and the fourth grain varies from h_{r4} to $(\sqrt{2})h - h_r$. For low coverage with $h \leq \bar{d}(2S_f)^{1/2}$ or $VS_f \leq (\pi/8)$, $\theta_{\min 1}$ is less than $\pi/4$, and the first case is accurate. It is also accurate for most regions with larger coverages but must be modified for the fraction of cases indicated. This allows for multiple overlap in the square arrangement and is thus an estimate of the true value of $C_1(h_r)$. Developed grains in the same half-layer are assumed not to overlap with one another; this assumption of linearity of VS_f is discussed above. Consider-

ing the unnormalized volume contribution,

$$P_V(\Delta x) = P(\Delta x)A[h_{r \min}(\Delta x)] \\ = A[h_{r \min}(\Delta x)](1 - 2|\Delta x - 0.5|), \quad (14a)$$

and summing over arcs of δh_r gives

$$\overline{C}_1(\Delta x) = \int_{h_r=h_{r \min}}^{(\sqrt{2})h} C_1(h_r)' \frac{-\delta A(h_r)}{\delta h_r} dh_r, \quad (14b)$$

From this the overall estimate of

$$C_1 = \frac{\int_0^1 P_V(\Delta x)\overline{C}_1(\Delta x)d\Delta x}{\int_0^1 P_V(\Delta x)d\Delta x} \quad (14c)$$

gives $C_1 \approx 0.08788$. The model dependence of this is small. As expected, the mean value for $\Delta x = 0$ of C_1 is 0, the mean value for $\Delta x = 0.5$ is 0.02056 (overlapping within a half-layer will lie between this and the mean for $\Delta x = 0.25$ of 0.000964), and the mean at the peak probability with $\Delta x = 0.725$ is 0.09344. Multiple overlap accounts for 1.8% of the value for $\Delta x = 1$, where C_1 reaches VS_f , and a larger percentage for smaller values of the depth separation. A similar estimate for C_2 ,

$$C_2 = \frac{\int_{0.5}^{1.5} P(\Delta x - 0.5)A[h_{r \min}(\Delta x)]\overline{C}_1(\Delta x)d\Delta x}{\int_{0.5}^{1.5} P(\Delta x - 0.5)A[h_{r \min}(\Delta x)]d\Delta x}, \quad (14d)$$

gives the direct overlap of the two layers, neglecting the arrangement of the intermediate layer. The correct value should lie between this lower limit and $C_2 = VS_f$. A scaling correction may be introduced,⁷ or an estimate of the parameter may be gained from

$$C_2 = \left[\int_{0.5}^{1.5} P(\Delta x - 0.5)A[h_{r \min}(\Delta x/2)] \right. \\ \left. \times (\overline{C}_1(\Delta x)A[h_{r \min}(\Delta x/2)] + VS_f\{A[h_{r \min}(\Delta x)] \right. \\ \left. - A[h_{r \min}(\Delta x/2)]\})d\Delta x \right] \\ \left/ \left\{ \int_{0.5}^{1.5} P(\Delta x - 0.5)A[h_{r \min}(\Delta x)] \right. \right. \\ \left. \left. \times A[h_{r \min}(\Delta x/2)]d\Delta x \right\}. \quad (14e)$$

This estimates the correlation of area occluded by the intermediate layer with locations of grains in adjacent layers. For $VS_f > (\pi/4)$ the location of the grain at the center of the square gives full coverage of area in a single layer, but this coverage occurs only for developed grains with $S_f \gg 1$. Here units are not spherical grains but extruded silver clusters; so the

Table 2. Optimized Coefficients for DEF Parameters

Fit	Model	% v/v	t_0 (μm)	T (μm)	t_b (μm)	d (μm)	ΔC_1	C_f	S_f	χ_r^2
1	Smooth	0.410	1.60	14.3	(185)	1.505	Δ^a	2.61	1.484	1.4
2	Smooth	0.3995	1.63	19.0	(185)	1.43	Δ^a	2.76	1.520	1.1
3	Smooth	0.3945	1.44	14.0	(185)	1.625	Δ^a	2.165	1.54	1.7
4	Smooth	0.398	1.505	15.5	(185)	1.525	Yes	2.225	2.19	1.9
5	Rough	0.400	1.525	15.0	(185)	1.655	Δ^a	1.875	1.521	2.6
6	Smooth	0.410	1.76	16.0	(185)	1.52	No	1.92	1.86	1.8
7	Smooth	0.4095	1.78	14.0	(185)	1.525	No	1.915	1.857	2.0
8	Smooth	0.4078	1.74	19.0	(185)	1.46	No	2.02	1.86	1.7

^aCoefficients adjusted (reduced) by 10%; see text.

correlation of adjacent and deeper layers approaches the uncorrelated estimate (VS_f). Accurate values for C_1 and C_2 should yield self-consistent recursion relations without transferral to uncorrelated estimates, if the resulting densities are finite and the total area is not occluded. This depends partly on higher-order correlation but may be used to adjust C_1 and C_2 from estimated values. For DEF undeveloped grains Eq. (14e) predicts $C_2 \approx 0.2966$, while adjustment in the range between the lower estimate and V yields $C_2 = 0.2972$ as the minimum value for which recursion is self-consistent. These two values are in good agreement with $V = 0.3$ and support the use of either method. For developed clusters ($S_f \approx$

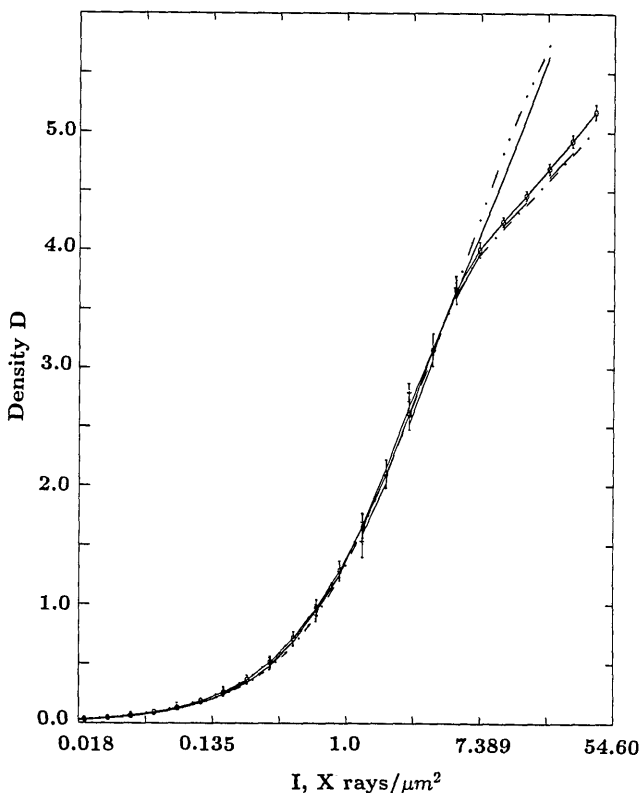
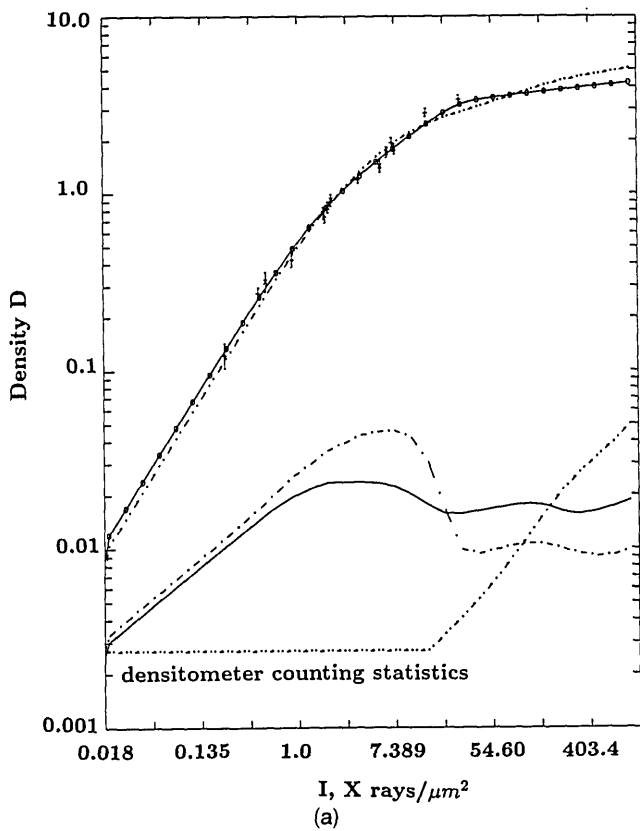
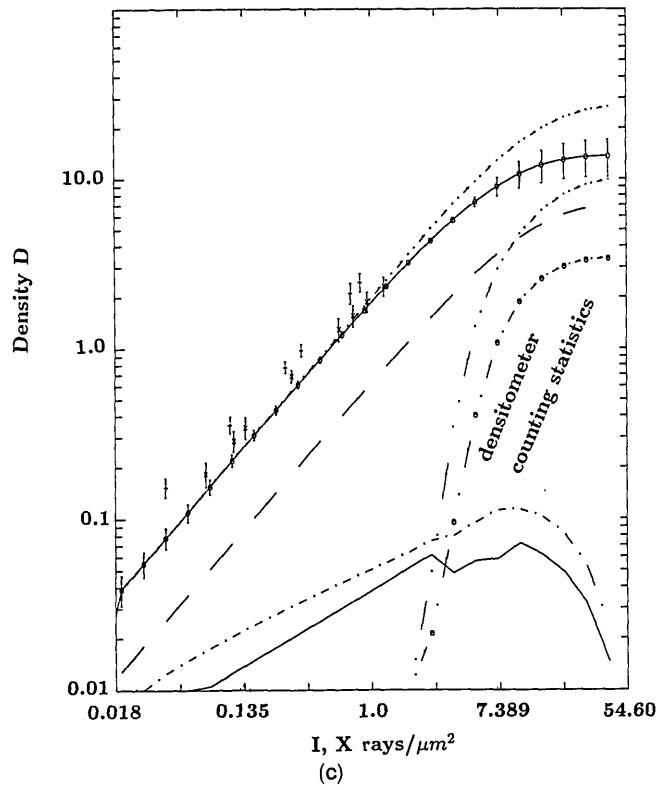


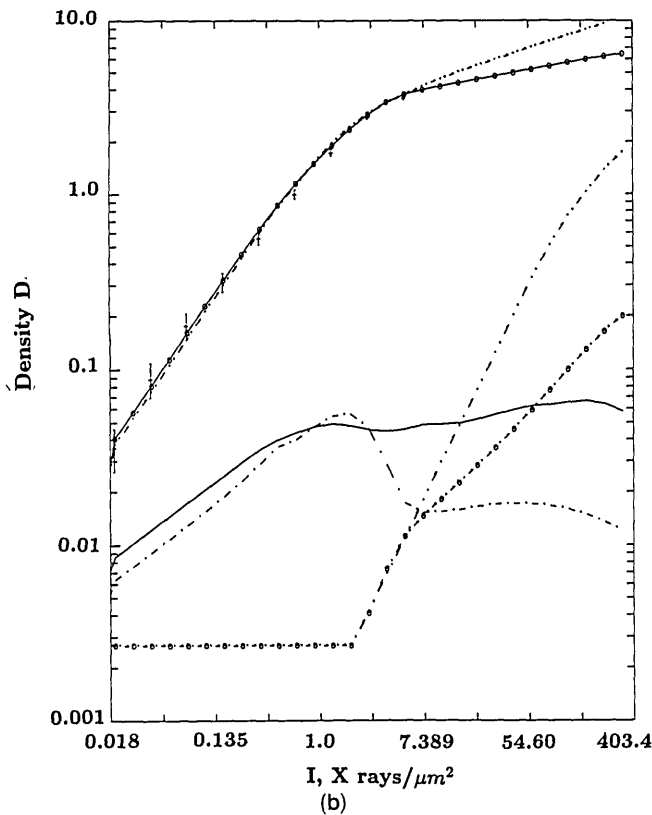
Fig. 3. $D - \ln I$ relation for DEF emulsion for 1.49-keV x rays. Data (+) are compared with the models in Table 2 with model 1, —○— (with uncertainty indicated); 2, —•—; 4, —•—; 5, —; and 6, —. Most models show a transition around $D = 4$ for this and other low energies, but all agree well with the data.



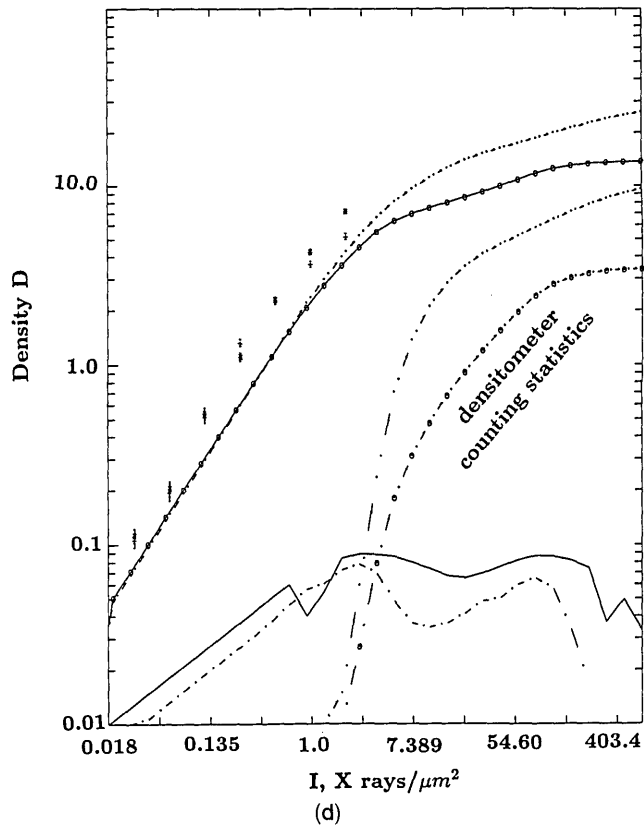
(a)



(c)



(b)



(d)

Fig. 4. $\ln D - \ln I$ relation for DEF emulsion. Data (+, x) are compared with model 1, —○—, which gives $\chi_r^2 = 1.4$ for all fitted data, and model 6, ···, with C_1 and C_2 unaltered and $\chi_r^2 = 1.8$. Uncertainties are presented with contributions from densitometer statistics (·-·, ○-○) depending on emulsion thickness and saturation density, while grain statistical contributions (·-·) and those for incident x-ray statistics (—) have weaker dependence on thickness, being dominated by upper layers. Results are presented for (a) 0.93-keV, (b) 1.74-keV, and (c) 8.05-keV energies that show data fitted by the model [except for + in (c)] and for (d) 4.51 + 4.93 + ... keV energies, which show corrected (+) and uncorrected (*) data that are not consistent with available models. (c) The contribution to density of the second emulsion for model 1 is given in (c) (·-·). The precision of recursion relations and truncation of correlated calculations can lead to small discontinuities in error from x-ray statistics, as in (c) and (d).

2) the range of C_2 between 0.531 and $V = 0.6$ is unable to give self-consistent recursion. Grain coefficients and saturation densities vary little in this range; thus estimates of $C_2 \approx 0.591$ from Eq. (14e) or $V = 0.6$ by iteration are equivalent.

This total occlusion or transferral to uncorrelated recursion equations results from C_1 being a coefficient for spherical grains rather than for extruded clusters, which are less correlated entities. In addition, arrangements of nearest-neighbor grains in triangular or paired arrangements can lead to slightly lower values of C_1 . C_1 estimates for grains and clusters are probably accurate to within 10%. While C_2 is adequate within the system of equations, C_1 is often an underestimate and may be adjusted so that it allows for this decrease in correlation. The maximum density obtained without adjusting C_1 provides an underestimate of the final saturation value, while the adjusted value can provide an overestimate. This provides a relatively narrow range of possible saturation densities. In general, and particularly for DEF emulsions, the former value is preferred. The calculation is made over more layers than actually exist, and the finite emulsion thickness limits further the difference between the two predictions.

Observed densities for low exposures can be understood only if $S_f > 1$ and $C_f > 1$. This confirms that the mean photographic unit is a clump of (two) adjacent physical grains, with a higher cross-sectional area; hence it is exposed more readily. It simultaneously occludes a larger fraction of available area, and development flattens and increases this coverage; so the density can be increased dramatically. S_f affects probabilities and V values only for the density sums, while C_f affects sums along x-ray and photon paths and changes G_{tot} and $G_{\text{tot}i}$ but has no effect on V .

7. X-Ray Counting Statistics

In CI we described the dominant contribution to x-ray counting statistics from the incident photons at the film after the supercoat. This is precise for the surface layer, but there will be fewer x rays incident on the last layer. Uncertainties at this depth are therefore underestimated if the earlier prescription is used but are readily corrected when the photons remaining at each depth are evaluated and errors are provided accordingly. Binomial errors at each depth should be added in quadrature with the effects of incident Poisson errors, but this procedure requires long calculations. A simple overestimate of this error source is obtained when we combine Poisson and binomial statistics to give a Poisson error for each half-layer, whose effects may then be added linearly.

8. Model Agreement for DEF Emulsion

Data for this thick emulsion film with an emulsion on each side of the substrate are obtained as we discussed in Section 1. In this paper substantial improvement over models of the preceding paper and over previous literature is shown. The lowest χ_r^2 of 2.2 was achieved only for the smooth integral model

with the addition of the semiempirical d_0 parameter. Here, the only result worse than this is for the (correlated) rough surface model, which as we explained above is inappropriate for DEF emulsions. The fourth fit quoted is qualitatively most similar to earlier integral models (with regard to the high-density behavior), since C_1 is distorted here to allow correlated calculation for all layers. The difference in χ_r^2 values between this and other smooth models indicates insensitivity of the model to precise values of C_1 and C_2 . This is also seen from fits with no modification of the coefficients.

Best fits are given with < 10% modification of silver cluster coefficients, as represented (for different parameters) in the first three rows of Table 2. This corresponds to the uncertainty in the calculation of C_1 and C_2 based on possible alternative nearest-neighbor geometries and the difference between cluster and grain occlusion. For the best fit with all parameters within physical limits, $\chi_r^2 = 1.4$. We may compare this with 1.7 (essentially without modification of parameters from earlier estimates) and 1.1 (by reducing d and increasing t_0 , T , and C_f above physical values). The three fits are barely indistinguishable below 4 keV but diverge particularly for 8.05 keV, for which model predictions are slightly low compared with data.

Agreement of experimental data with model predictions within 1.4 standard deviations may be taken as verification of the model and experimental uncertainties used. Quoted uncertainties should in all cases be greater than error estimates from x-ray, grain, and photon-counting sources, since the latter do not include background and diffuse-specular conversion estimates. This is seen in all data sets. The expected smooth $D - \ln I$ relation is predicted for high energies, but a sharper transition is observed at lower energies for most fits because of the correlation and the second emulsion (Fig. 3). We used the $\chi_r^2 = 1.8$ fit with no modification of C_1 and C_2 coefficients in Fig. 4, and model 1 where these are shifted within estimated uncertainties, to estimate the uncertainty within the model for the data. The component resulting from photon statistics is as defined in CI but without reduction of the expression to the lower-intensity approximation. The behavior of grain and x-ray errors with D is different at low energies from that depicted in CI. X-ray uncertainties include additional terms and are larger here.

Grain errors are similar but are reduced up to intensities at which peak errors are observed (i.e., over the region where grain errors dominate over

Table 3. Optimized Coefficients for 101 Parameters

Model	%v/v	t_0 (μm)	T (μm)	d (μm)	ΔC_1	C_f	S_f	χ_r^2
Rough	0.74	0.053	1.2	0.85	No	1.34	1.36	6.7
Rough	0.725	0.053	1.2	0.87	No	1.29	1.383	6.7
Rough, Eq. (25c) ^a	0.74	0.052	Mono	0.915	No	1.27	1.535	7.4

^aRef. 8.

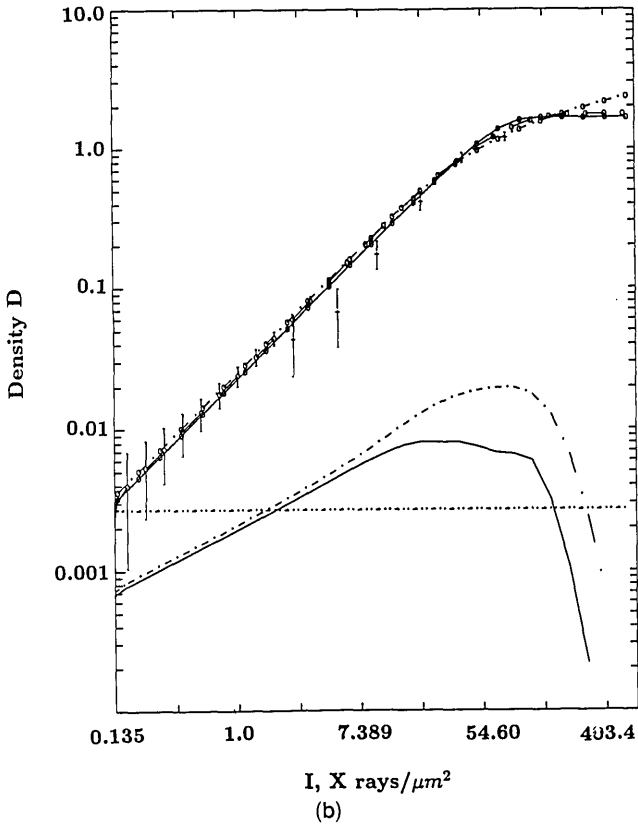
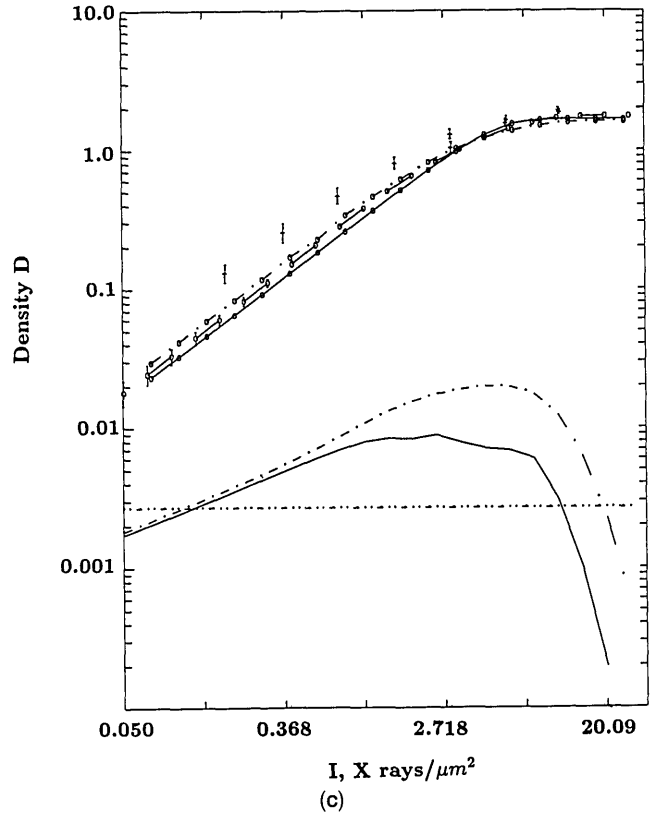
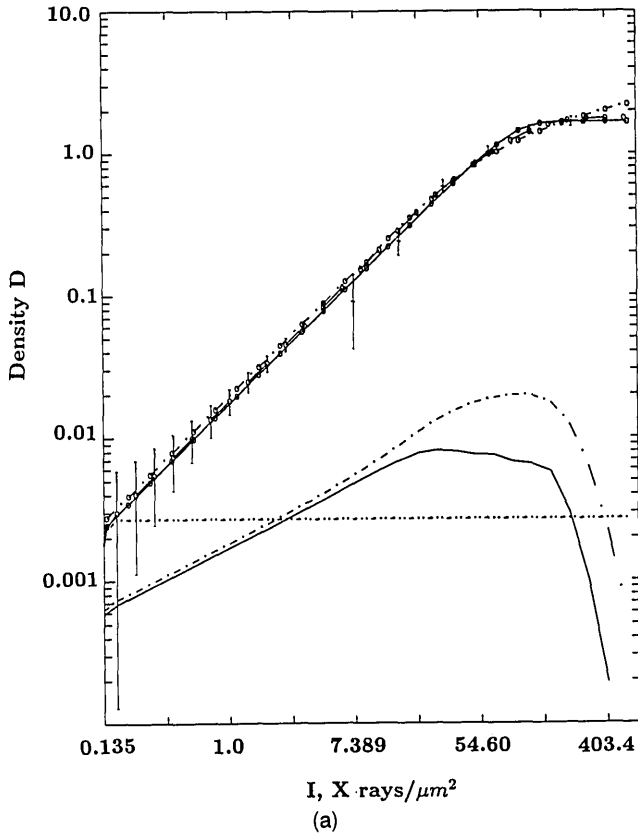


Fig. 5. Simple density estimates and density errors versus $\ln I$ for 101 emulsion using the rough emulsion model of this paper (O-O) with errors, compared with CI (—O— and O—O) and experiment (+) for (a) 9.508 eV, (b) 16.869 eV, and (c) 524.9 eV. Error contributions from grain sources (—) exceed those from incident x-ray (—) sources. Detector photon counting and background uncertainty (indicated by “— and estimated data errors) can dominate at low and high densities.

other error sources) but decline significantly above this to a lower oscillating plateau. Results for 4.51 keV show a double peak resulting from saturation of the first and second emulsion, respectively, but the two peaks merge before 8.05-keV energies are attained.

Parameters suggest values of $\%v/v$ higher than expected, but the experimental determination assumed uncorrelated layer attenuation and is in agreement with the quoted value. In particular, attenuation is near μ_0 for the first layer of the emulsion and increases only slowly to μ' , so that observed attenuation relates to a mean over a finite emulsion and not to the limiting value (see CI). S_f indicates less significant expansion during development than integral model predictions, while C_f is similar to previous estimates. The trend to higher T , lower \bar{d} , and higher C_f is correlated so that $\sigma = C_f(\pi/4)\bar{d}^2$ is preserved while the number of half-layers $n = 2T/\bar{d}$ is increased. This would be expected if clusters were oblate spheroids leading to a shorter correlation or grain depth with a larger cross section per unit. The data set for 8.05 keV shows substantial improvement with these distortions, but it is also the only set where deep layers contribute or where the second emulsion contributes. Thus apparent oblateness or clustering, suggested by C_f , may actually relate to attenuation and correlation inadequacies of the model for deep layers or for the second emulsion. Correlated recursion relations transfer to uncorrelated equivalents for deep layers, as discussed. This could explain the observed distortion.

The systematic effects above are small and do not seriously impair the predictive capability of the model. Similar but larger systematics have been observed in other models and in the literature. Models diverge less at high densities than equivalent integral models and may be preferred as reliable estimators in these regions and in extrapolations to higher or lower energies.

9. Model Agreement for 101 Emulsion

Data are obtained from Refs. 10 and 13 as indicated in Section 1. For thin emulsions such as 101, the correlation parameters have less significance, and integral methods reduce to simple summations over layers. The main developments in the current models are that summation is consistently used for all emulsion thicknesses, summation is over half-layers rather than layers, and coverages will be modulated by C_1 correlation factors. This is shown in Table 3 to lead to a significant but small improvement of χ_r^2 values, while the rough surface integral model with an additional semiempirical parameter still has the best χ_r^2 . Parameters and fits (such as in Fig. 5) are similar to those presented in CI but with lower values for S_f . With this prescription for errors, contributions from grain and incident x-ray sources are equally important at low densities; they peak similarly but with grain contributions exceeding x-ray

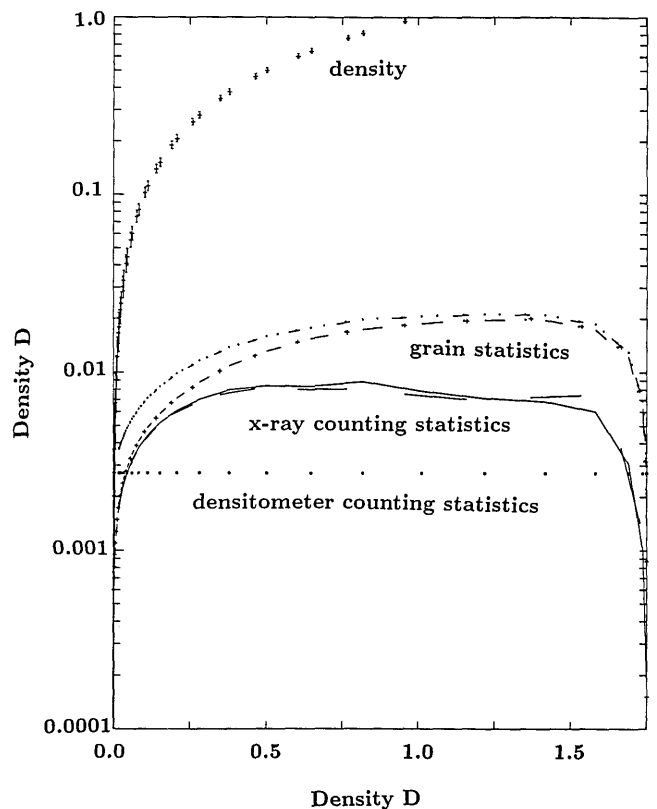


Fig. 6. Error contributions for 101 emulsion from densitometer photon statistics (*), x-ray counting errors (--- and — for 5.254 and 524.9 eV), and grain contributions (·—, +) to total uncertainty (·—) in D (+) versus D , which show strongly reduced dependence on energy, as opposed to models from CI.

counting contributions. Errors have little dependence on energy (Fig. 6), as opposed to simpler predictions from models of CI. Compared with these integral models, uncertainties are greater at low densities and lower at high densities. The magnitude at low densities is in agreement with experimental measurements of granularity.¹³

Agreement is limited by the quality and consistency of experimental data, especially at high densities where adjacent energies from the same source differ anomalously. This suggests that estimated errors are low by a factor of 2 or so, that there is significant variation in D - I relations between different batches of 101 emulsion, and that experiments duplicating and extending data sets for these and intermediate energies are required.

10. Conclusions

Values of C_f suggest a shape effect (i.e., nonsphericity or a grain size distribution) that is larger for DEF than 101 emulsions together with some distortion of values caused by imprecision of overlap coefficients and correlation of fitting parameters.

The purpose of this development has been in part to understand the physical processes taking place during photographic exposure and development and the shifts of densities with different energies, expo-

tures, and angles. A second motivation was to be able to derive believable and reliable estimates of statistical error for each intensity (and each channel in linearized spectra) so that fitted errors may be understood better and so that fits may use optimized (and valid) weighting schemes. In the process results pertaining to C_f , S_f , d_0 , d , α , and b have been obtained, and a simple summation model for grain distribution has been shown to be inadequate. Experimental effects in estimating converted specular densities and uncertainties have been noted.

Detailed models based on the integral approach to the equations have general validity and explain the shape and form of the characteristic curve for high- and low-energy x rays, particularly for thin emulsions with an empirical parameter that allows for initial layers. Models allowing for correlated sums over half-layers fit the available data for thick emulsions with $\chi^2 \approx 1$ and have the same number of free parameters as earlier models, with reasonable parameter values. Further investigation of correlated overlap coefficients may limit uncertainties in C_1 and C_2 to below current estimates of 10%. Further experiments should be performed for 101 and DEF emulsions, particularly at high and intermediate energies. Compared with earlier work, the current models may be more reliably extrapolated and interpolated from data to different energies, angles, and densities.

The author thanks Shell Australia, the Hasselblad Foundation, and the Draper's Company for support of this research and St. Anne's College, Oxford, for a Junior Research Fellowship covering part of the period of research. Acknowledgments go to J. D. Silver, D. D. Dietrich, and J. M. Laming for assistance and support, especially on the experimental side.

References

1. D. B. Brown, J. W. Criss, and L. S. Birks, "Sensitivity of x-ray films. I. A model for sensitivity in the 1–100 keV region," *J. Appl. Phys.* **47**, 3722–3731 (1976).
2. C. M. Dozier, D. B. Brown, L. S. Birks, P. B. Lyons, and R. F. Benjamin, "Sensitivity of x-ray film. II. Kodak no-screen film in the 1–100 keV region," *J. Appl. Phys.* **47**, 3732–3739 (1976).
3. W. C. Phillips, and G. N. Phillips, Jr., "Two new x-ray films: conditions for optimum development and calibration of response," *J. Appl. Crystallogr.* **18**, 3–7 (1985).
4. A. Poquérousse, "Réponse du film SB aux rayons X de 0,1 à 10 keV," *Rev. Phys. Appl.* **23**, 963–969 (1988).
5. P. D. Rockett, C. R. Bird, C. J. Hailey, D. Sullivan, D. B. Brown, and P. G. Burkhalter, "X-ray calibration of Kodak direct exposure film," *Appl. Opt.* **24**, 2536–2542 (1985).
6. B. L. Henke, S. L. Kwok, J. Y. Uejio, H. T. Yamada, and G. C. Young, "Low-energy x-ray response of photographic films. I. Mathematical models," *J. Opt. Soc. Am. B* **1**, 818–827 (1984).
7. C. T. Chantler, "Beam-foil spectroscopy of highly-ionized atoms, precision measurements of hydrogenic Lamb shifts and x-ray diffraction of curved crystals," D.Phil. thesis. (University of Oxford, Oxford, 1990), Chap. 4.
8. C. T. Chantler, "Photographic response to x-ray irradiation. I: Estimation of the photographic error statistic and development of analytic density-intensity equations," *Appl. Opt.* **32**, 2371–2397 (1993).
9. C. T. Chantler, J. D. Silver, and D. D. Dietrich, "Photographic response to x-ray irradiation. III: Photographic linearization of beam-foil spectra," *Appl. Opt.* **32**, 2411–2421 (1993).
10. B. L. Henke, F. G. Fujiwara, M. A. Tester, C. H. Dittmore, and M. A. Palmer, "Low-energy x-ray response of photographic films. II. Experimental characterization," *J. Opt. Soc. Am. B* **1**, 828–849 (1984).
11. B. L. Henke, J. Y. Uejio, G. F. Stone, C. H. Dittmore, and F. G. Fujiwara, "High-energy x-ray response of photographic films: models and measurement," *J. Opt. Soc. Am. B* **3**, 1540–1550 (1986).
12. C. E. K. Mees, *The Theory of the Photographic Process* (Macmillan, New York, 1946).
13. W. M. Burton, A. T. Hatter, and A. Ridgeley, "Photographic sensitivity measurements in the vacuum ultraviolet," *Appl. Opt.* **12**, 1851–1857 (1973).